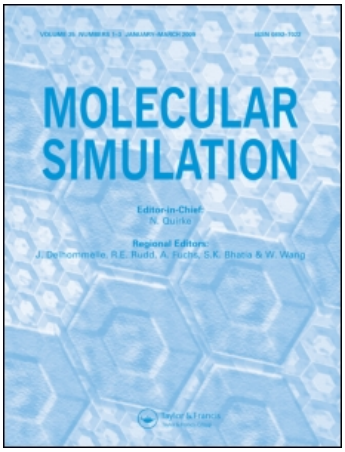

Molecular Simulation
Publication details, including instructions for authors and subscription information:
http://www.informaworld.com/smpp/title~content=t713644482

A Two-Ellipsoid Model Based Upon A Gaussian Overlap Potential

Jeong Geun Yoo[a]; Yoon Sup Lee[a]
[a] Department of Chemistry and Center for Molecular Science, Korea Advanced Institute of Science and Technology, Taejon, Republic of Korea

To cite this Article Yoo, Jeong Geun and Lee, Yoon Sup(1997) 'A Two-Ellipsoid Model Based Upon A Gaussian Overlap Potential', Molecular Simulation, 19: 2, 93 — 116
To link to this Article: DOI: 10.1080/08927029708024142
URL: http://dx.doi.org/10.1080/08927029708024142

Molecular Simulation, 1997, Vol. 19, pp. 93–116
Reprints available directly from the publisher
Photocopying permitted by license only

A TWO-ELLIPSOID MODEL BASED UPON A GAUSSIAN OVERLAP POTENTIAL

JEONG GEUN YOO and YOON SUP LEE

Department of Chemistry and Center for Molecular Science, Korea Advanced Institute of Science and Technology, Taejon, 305-701, Republic of Korea

(Received November 1996; Accepted January 1997)

The two-ellipsoid model (TEM) is proposed as a versatile single-site model which can be used in the study of liquid crystal phases. This TEM uses two ellipsoids to describe a molecule, one ellipsoid for the geometry and the other for the interaction strengths of the molecule. The present TEM can mimic asymmetric interactions of a liquid crystal molecule by separating the center of the interaction ellipsoid from that of the geometry ellipsoid. The potential energy surfaces of the present TEMs compare favorably with those of the corresponding Gay-Berne and the site–site models.

Monte Carlo simulations with 320 particles are performed for a symmetric interaction TEM and an asymmetric interaction TEM. The asymmetric interaction TEM displays a slightly higher transition temperature than the symmetric interaction TEM indicating that asymmetric interactions can be a driving force in a phase transition. Radial and cylindrical distribution functions of two models in the isotropic phase are similar, but those in the nematic phase are quite different.

Keywords: Modified Gay-Berne model; asymmetric interactions; liquid crystal; nematic phase Monte Carlo simulation; Gaussian overlap potential

1. INTRODUCTION

Computer simulation methods such as the Monte Carlo method (MC) or Molecular Dynamics (MD) are frequently used for the study of liquid crystal phases since those methods allow, with only a few approximations, to derive bulk properties from microscopic models. Microscopic models that have been used for liquid crystals are numerous, and may be classified, in

decreasing order of complexity, as the full atomic models [1], united atomic models [1–5], site–site models [6, 7] and single-site models [8–15]. Single-site models are widely used in the simulations due to computational efficiency. Although single-site models are the crudest microscopic models, it is still possible to include most of qualitatively important interactions in the models.

Gay and Berne proposed a single-site model [11] as a modification of the earlier Gaussian overlap model of Berne and Pechukas [16]. This model of Gay and Berne has been widely applied to the study of liquid crystal phases because this model with a single interaction center mimics the site–site model quite well. The Gaussian overlap model first reported by Berne and Pechukas [16], had unrealistic interactions, but Gay and Berne improved the model significantly by using a modified interaction potential, fitting parameters and a shifted Lennard-Jones(LJ) potential. Berne and Pechukas generated two parameters, one for the range and the other for the strength, with only one ellipsoid representing a molecule. The interaction strength at a fixed $\mathbf{u}_1 \cdot \mathbf{u}_2$ is the same regardless of the relative positions of two centers, producing too unrealistic potentials [16]. In this paper, we propose and test a two-ellipsoid model (TEM) in which an additional ellipsoidal Gaussian describing anisotropic interactions is introduced to extend the Gaussian overlap concept to the anisotropic interaction. In TEM the range parameter is obtained from the same scheme as the Berne-Pechukas model from the ellipsoid representing molecular geometry, but the strength parameter is obtained from the overlap between Gaussians representing the intermolecular interactions at the optimum distance of a shifted LJ potential. Even when a liquid crystal molecule can be considered to be symmetric along the major axis partially due to the rapid rotation, the center of inversion is usually lacking along the major axis. The present TEM can describe the lack of central symmetry in liquid crystal molecules by shifting the center of interaction ellipsoid from that of geometry ellipsoid along the major axis. The asymmetric two-ellipsoid model (ATEM) is the first Gaussian overlap model, to the best of our knowledge, to depict molecules without a center of symmetry. We expect that the asymmetric interactions may affect various liquid crystalline properties such as double layered smectic phase, reentrance effect and surface pretilt angle. When the centers of geometry and interaction are defined to be same in TEM, we obtain a symmetric two-ellipsoid model (STEM) which is similar to a Gay-Berne model. STEM and ATEM are described and compared with corresponding site–site models in the next section. NVT MC calculations have been performed using TEMs and results are discussed in the following section.

2. MODEL POTENTIAL

A. Two-Ellipsoid Model

There are two parameters in the LJ potential, σ for the range and ε for the strength. For an elongated structure, these parameters can be modified to reflect anisotropy in geometry and interactions. Berne and Pechukas proposed a Gaussian overlap model [16] to determine orientation dependent range and strength parameters. In this model, the range parameter $\sigma(\mathbf{u}_1, \mathbf{u}_2, \hat{\mathbf{r}})$ describes anisotropic geometry, but the strength parameter $\varepsilon(\mathbf{u}_1, \mathbf{u}_2)$ does not describe anisotropic interactions. Gay and Berne modified the strength parameter to mimic anisotropic interactions by introducing an additional term similar to $1/\sigma^2$ and parameters ν and μ. The potential of Gay and Berne [11] is

$$V(\mathbf{u}_1, \mathbf{u}_2, \hat{\mathbf{r}}) = 4\varepsilon(\mathbf{u}_1, \mathbf{u}_2, \hat{\mathbf{r}}) \left[\left(\frac{\sigma_0}{r - \sigma(\mathbf{u}_1, \mathbf{u}_2, \hat{\mathbf{r}}) + \sigma_0} \right)^{12} - \left(\frac{\sigma_0}{r - \sigma(\mathbf{u}_1, \mathbf{u}_2, \hat{\mathbf{r}}) + \sigma_0} \right)^{6} \right] \tag{1}$$

$$\sigma(\mathbf{u}_1, \mathbf{u}_2, \hat{\mathbf{r}}) = \sigma_0 \left(1 - \frac{x}{2} \left[\frac{(\hat{\mathbf{r}} \cdot \mathbf{u}_1 + \hat{\mathbf{r}} \cdot \mathbf{u}_2)^2}{1 + x(\mathbf{u}_1 \cdot \mathbf{u}_2)} + \frac{(\hat{\mathbf{r}} \cdot \mathbf{u}_1 - \hat{\mathbf{r}} \cdot \mathbf{u}_2)^2}{1 - x(\mathbf{u}_1 \cdot \mathbf{u}_2)} \right] \right)^2 \tag{2}$$

$$\varepsilon(\mathbf{u}_1, \mathbf{u}_2, \hat{\mathbf{r}}) = \varepsilon^{\nu}(\mathbf{u}_1, \mathbf{u}_2)\, \varepsilon'^{\mu}(\mathbf{u}_1, \mathbf{u}_2, \hat{\mathbf{r}}) \tag{3}$$

$$\varepsilon(\mathbf{u}_1, \mathbf{u}_2) = \varepsilon_0 [1 - x^2 (\mathbf{u}_1 \cdot \mathbf{u}_2)^2]^{-1/2} \tag{4}$$

$$\varepsilon'(\mathbf{u}_1, \mathbf{u}_2, \hat{\mathbf{r}}) = 1 - \frac{x'}{2} \left[\frac{(\hat{\mathbf{r}} \cdot \mathbf{u}_1 + \hat{\mathbf{r}} \cdot \mathbf{u}_2)^2}{1 + x'(\mathbf{u}_1 \cdot \mathbf{u}_2)} + \frac{(\hat{\mathbf{r}} \cdot \mathbf{u}_1 - \hat{\mathbf{r}} \cdot \mathbf{u}_2)^2}{1 - x'(\mathbf{u}_1 \cdot \mathbf{u}_2)} \right] \tag{5}$$

$$x = (\sigma_{\parallel}^2 - \sigma_{\perp}^2)/(\sigma_{\parallel}^2 + \sigma_{\perp}^2) \tag{6}$$

$$x' = (\varepsilon_s^{1/\mu} - \varepsilon_e^{1/\mu})/(\varepsilon_s^{1/\mu} + \varepsilon_e^{1/\mu}) \tag{7}$$

where Eq. (1) is a shifted LJ potential. The anisotropic interaction can be represented by $\varepsilon'(\mathbf{u}_1, \mathbf{u}_2, \hat{\mathbf{r}})$ and the flexibility of anisotropic interactions can be achieved by parameters ν and μ. The Gay-Berne potential is a well-contrived single-site potential and is frequently used for the study of liquid

crystals [9, 10, 13] although the strength parameter of this model does not obey the Gaussian overlap concept.

In the present TEM, an additional ellipsoidal Gaussian representing interaction is introduced to expand the Gaussian overlap concept to anisotropic interactions. The range parameter, $\sigma(\mathbf{u}_1, \mathbf{u}_2, \hat{\mathbf{r}})$, is obtained from the geometry ellipsoidal Gaussian in the same manner as the Berne-Pechukas model. The strength parameter $\varepsilon(\mathbf{u}_1, \mathbf{u}_2, \hat{\mathbf{r}})$ is proportional to the overlap between two interaction ellipsoidal Gaussians at the optimum distance of geometry ellipsoidal Gaussians.

In Figure 1(a), the large ellipsoidal structure represents the geometry of a liquid crystal molecule and the small structure represents the interaction strength of the molecule. $\mathbf{u}_i$ is the unit vector of the major axis of particle i, and $\hat{\mathbf{r}}$ is the unit vector joining two centers of geometry ellipsoids. The shifted LJ potential and the range parameter, $\sigma(\mathbf{u}_1, \mathbf{u}_2, \hat{\mathbf{r}})$, are defined by Eq (1) and Eq (2), respectively.

The optimum distance in the shifted LJ potential of Eq (1) is given by

$$\sigma_{eq}(\mathbf{u}_1, \mathbf{u}_2, \hat{\mathbf{r}}) = \sigma(\mathbf{u}_1, \mathbf{u}_2, \hat{\mathbf{r}}) + (2^{(1/6)} - 1)\sigma_0 \tag{8}$$

The strength $\varepsilon(\mathbf{u}_1, \mathbf{u}_2, \hat{\mathbf{r}})$ is defined to be proportional to the overlap between two Gaussians of interaction ellipsoids at the separation of $r_e(\mathbf{u}_1, \mathbf{u}_2, \hat{\mathbf{r}})$ when

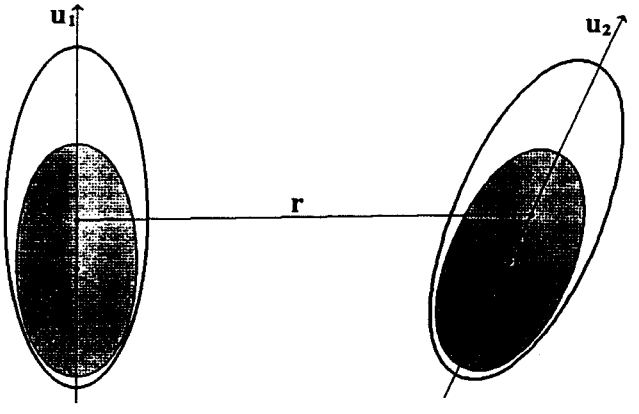

a

FIGURE 1 Schematic representation of TEM. $\mathbf{u}_1$ and $\mathbf{u}_2$ are unit vectors of major axes of particle 1 and 2. respectively, $\mathbf{r}$ is the vector joining the centers of geometric ellipsoids 1 and 2. The range parameter is calculated from the orientation of geometric ellipsoids (larger ellipsoids) and the strength parameter is calculated from the Gaussian overlap quantities of interaction ellipsoids (smaller shaped ellipsoids) at the optimum distance along the vector $\mathbf{r}$ (b).

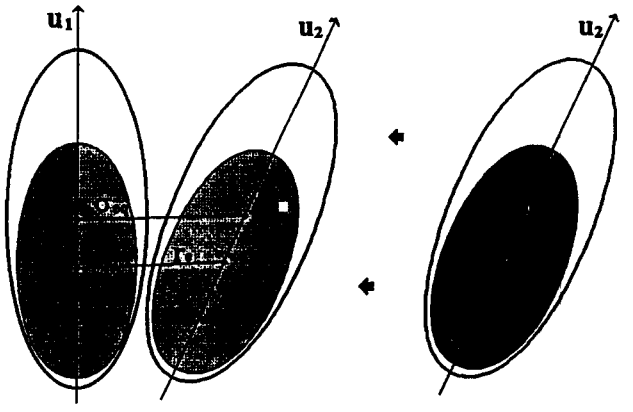

b

FIGURE 1 (*Continued*).

$\hat{\mathbf{r}}_e$ is the unit vector joining two centers of interaction ellipsoids at the optimum distance of the geometry ellipsoid $\sigma_{eq}(\mathbf{u}_1, \mathbf{u}_2, \hat{\mathbf{r}})$ (Fig. 1(b)). Then the strength parameter of TEM can be expressed as

$$\varepsilon(\mathbf{u}_1, \mathbf{u}_2, \hat{\mathbf{r}}) = \varepsilon_e(\mathbf{u}_1, \mathbf{u}_2) \exp[-r_e(\mathbf{u}_1, \mathbf{u}_2, \hat{\mathbf{r}})^2/\sigma_e(\mathbf{u}_1, \mathbf{u}_2, \hat{\mathbf{r}})^2] \tag{9}$$

$$\sigma_e(\mathbf{u}_1, \mathbf{u}_2, \hat{\mathbf{r}}_e) = \sigma_{e0}\left(1 - \frac{x'}{2}\left[\frac{(\hat{\mathbf{r}}_e \cdot \mathbf{u}_1 + \hat{\mathbf{r}}_e \cdot \mathbf{u}_2)^2}{1 + x'(\mathbf{u}_1 \cdot \mathbf{u}_2)} + \frac{(\hat{\mathbf{r}}_e \cdot \mathbf{u}_1 - \hat{\mathbf{r}}_e \cdot \mathbf{u}_2)^2}{1 - x'(\mathbf{u}_1 \cdot \mathbf{u}_2)}\right]\right)^2 \tag{10}$$

$$\varepsilon_e(\mathbf{u}_1, \mathbf{u}_2) = \varepsilon_{e0}[1 - x'^2(\mathbf{u}_1 \cdot \mathbf{u}_2)^2]^{(-1/2)} \tag{11}$$

$$x' = (\sigma_{e\parallel}^2 - \sigma_{e\perp}^2)/(\sigma_{e\parallel}^2 + \sigma_{e\perp}^2) \tag{12}$$

where $\sigma_{e0} = \sqrt{2}\sigma_{e\perp}$, $\sigma_{e\parallel}$ is the length of the major axis of an interaction ellipsoid, and $\sigma_{e\perp}$ is the length of the minor axis of an interaction ellipsoid. When the above $\sigma(\mathbf{u}_1, \mathbf{u}_2, \hat{\mathbf{r}})$ and $\varepsilon(\mathbf{u}_1, \mathbf{u}_2, \hat{\mathbf{r}})$ are applied to the shifted LJ potential of Eq. (1), the potential having anisotropic interaction and anisotropic geometry can be defined.

Most molecules having the nematic liquid crystal phase have anisotropy in molecular shapes and interactions. For an the idealized molecule X - B - A - B' - Y, where X and Y are terminal groups, B and B' are rings and A is a linking group, the shape may be regarded as a rod. In a single-site model, the above molecule can be modeled as a sphero-cylinder or an ellipsoid. In common liquid crystal molecules, terminal groups X and Y are different and sometimes B and B' also are different ring groups. Although it is reasonable to assume the symmetric molecular shape along the major axis

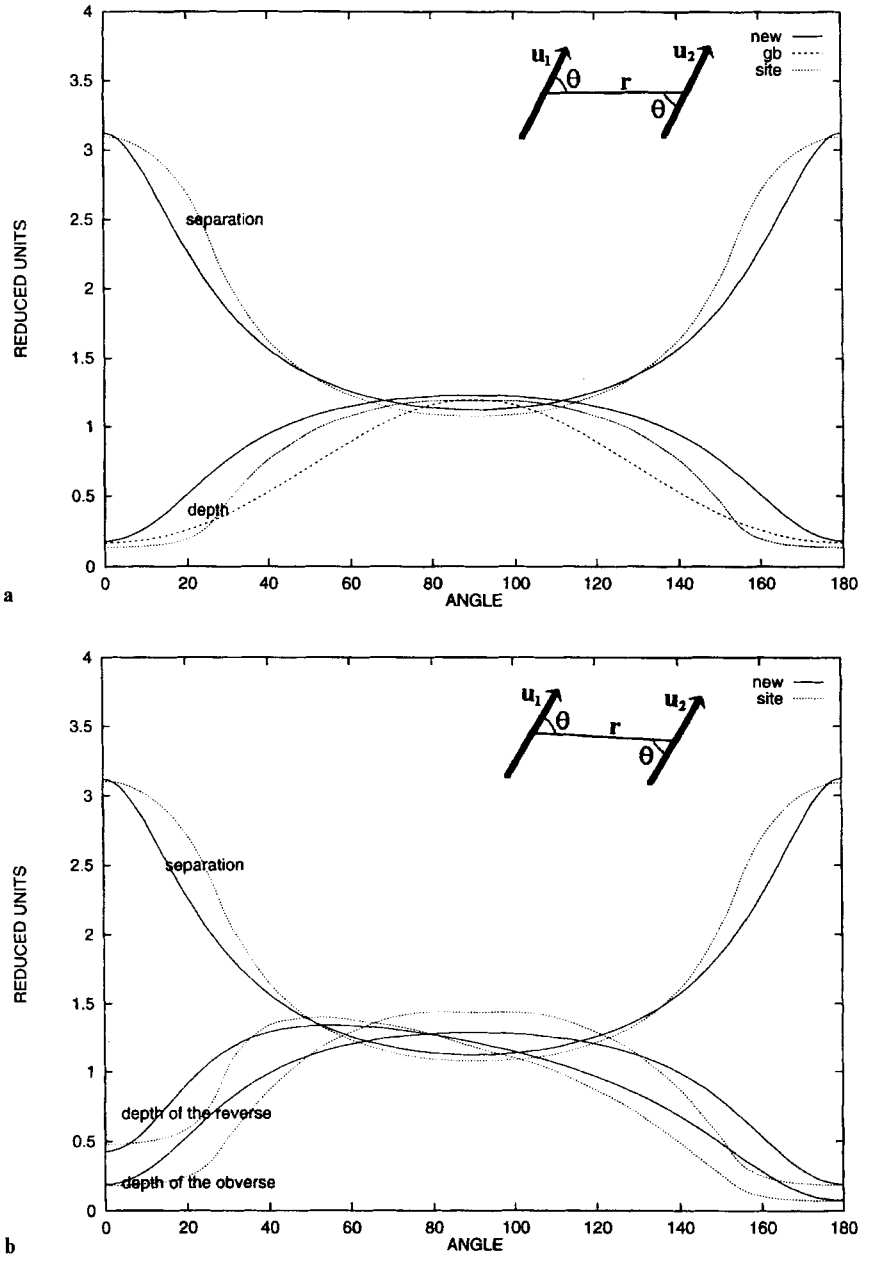

FIGURE 2 Comparison of the maximum well depths and separations at maximum well depths for the in-plane conrotatory movement. The site–site model (dotted line), the Gay-Berne model (dashed line) and the TEM (solid line) are shown. The unit of the separation is σ_0 and the unit of the maximum well depth is ε_*. (a) is for the STEM and (b) for the ATEM. where the observe means that major axes of particle 1 and 2 turn in direction of the arrow, and the reverse means the major axis of particle 2 turns in an opposite direction from the obverse configuration.

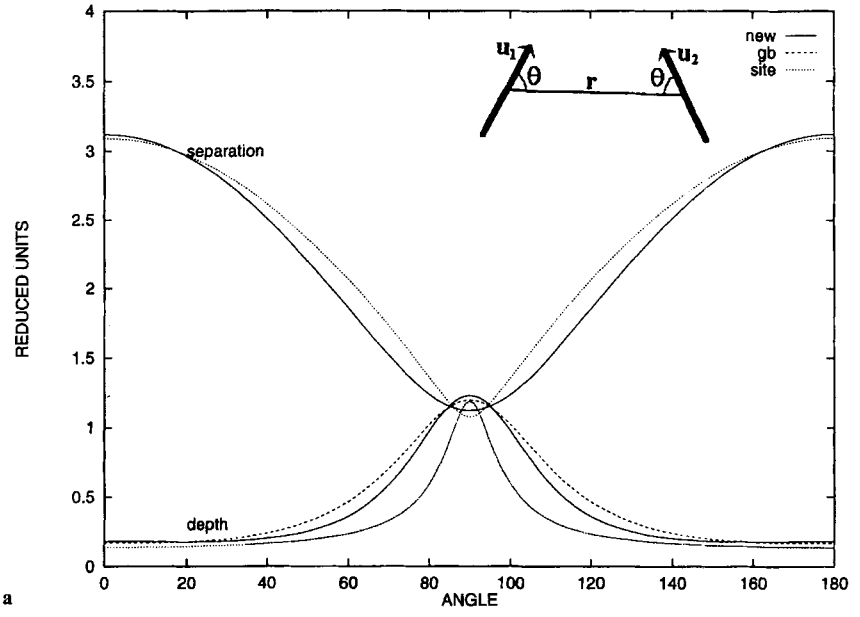

a

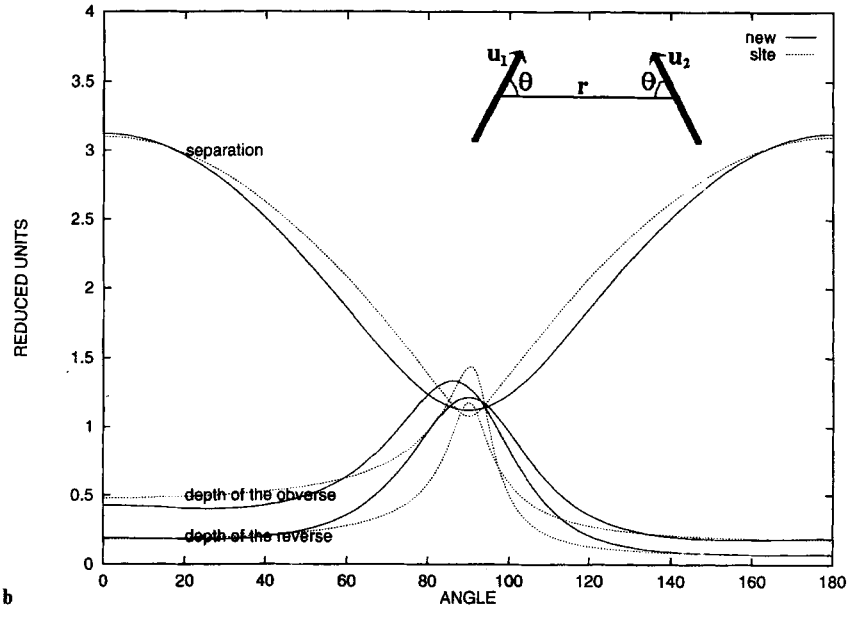

b

FIGURE 3 Comparison of the maximum well depths and separations at maximum well depths for the in-plane disrotatory movement. (a) is for the STEM, and (b) for the ATEM. All definitions and notations are same as in Figure 2.

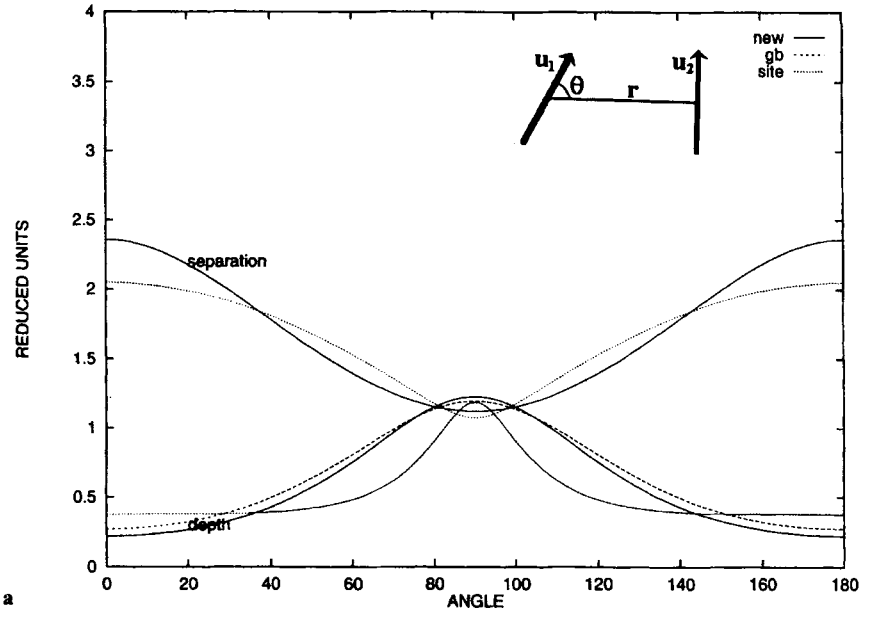

a

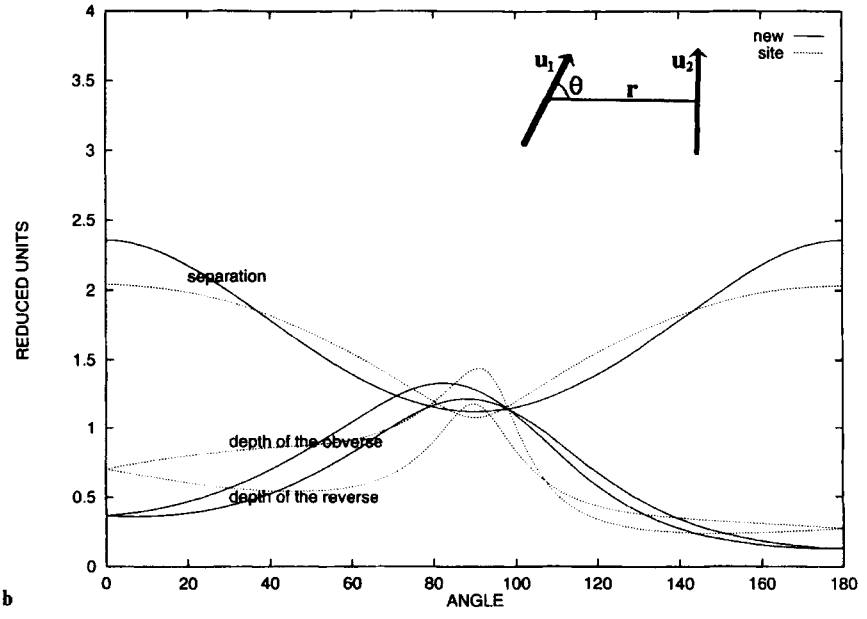

b

FIGURE 4 Comparison of the maximum well depths and separations at maximum well depths for the in-plane rotation of $\mathbf{u}_1$ with $\mathbf{u}_2$ fixed at a position perpendicular to $\mathbf{r}$. (a) is for the STEM, and (b) for the ATEM. All definitions and notations are same as in Figure 2.

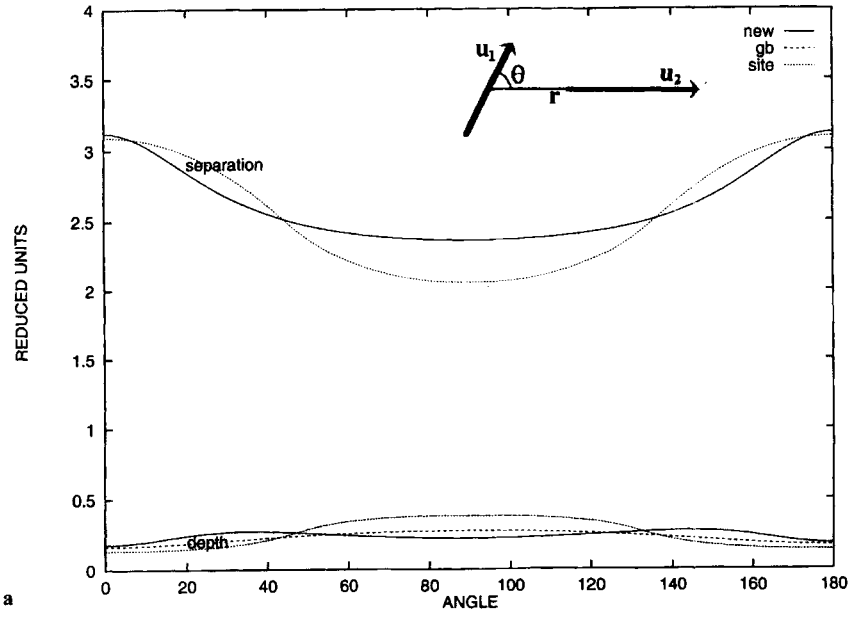

a

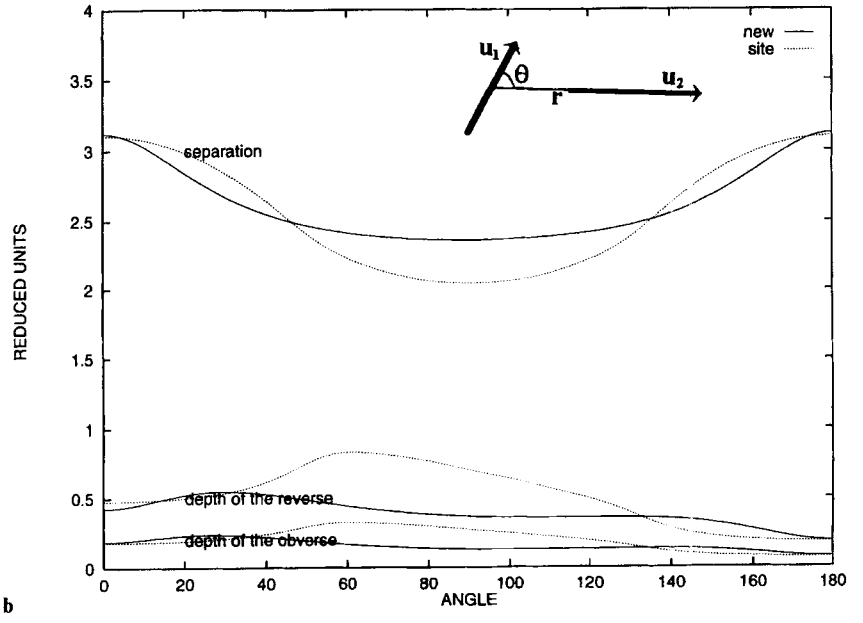

b

FIGURE 5 Comparison of the maximum well depths and separations at maximum well depths for the in-plane rotation of $\mathbf{u}_1$ with $\mathbf{u}_2$ fixed at a position parallel to $\mathbf{r}$. (a) is for the STEM, and (b) for the ATEM. All definitions and notations are same as in Figure 2.

such as a sphero-cylinder or ellipsoid in the model, assuming the symmetric interaction along the major axis may not be adequate. For example, in the 5CB molecule, X is $CH_2CH_2CH_2CH_2CH_3$. Y is CN, and B - A - B' is biphenyl. The structure of this molecule can be reasonably modeled by a symmetric structure as long as the center of the model is shifted somewhat toward X from A. The interactions are not properly described by the same symmetric model since the center of the interaction shape must be shifted toward Y from the center of structure. Therefore, it is useful to have asymmetric interaction model along the major axis by separating centers of interaction from that of the geometry. In this paper, we set both the molecular structure and the interaction shape to be ellipsoids in order to reflect the dependence of interactions on the molecular structure. The asymmetric interaction along the major axis is mimiced by shifting the center of the ellipsoid representing the molecular interaction by some distances along the major axis from the center of the ellipsoid representing the molecular structure. This model is ATEM and shown in Figure 1. As was mentioned earlier, STEM is obtained when the centers of the interaction ellipsoid and the geometry ellipsoid coincide.

For a STEM and a ATEM, the maximum well depth $\varepsilon(\mathbf{u}_1, \mathbf{u}_2, \hat{\mathbf{r}})$ and the separation at maximum well depth $\sigma_{eq}(\mathbf{u}_1, \mathbf{u}_{22}, \hat{\mathbf{r}})$ at several pair orientations are displayed in Figure 2 to Figure 5. The results of the STEM are compared with those of the Gay-Berne model and the site–site model. The values of the ATEM are compared only with those of the asymmetric site–site model because the Gay-Berne model does not treat asymmetric interactions along the major axis. The site–site model with 5 interaction centers and $\sigma_{\parallel}/\sigma_{\perp} = 3$ is selected as the standard and sketched in Figure 6. The potential function of the site-site model is

$$V(i,j) = \sqrt{\varepsilon_i \cdot \varepsilon_j}\,[(\sigma/r_{i,j})^{12} - (\sigma/r_{i,j})^6]. \tag{13}$$

Parameters of the TEMs used in the present study are listed in Table I, and corresponding parameters of the Gay-Berne model and the site–site models

TABLE I Parameters of TEMs

	Symmetric	*Asymmetric*
$\sigma_{\perp}$	1.00	1.00
$\sigma_{\parallel}$	3.00	3.00
$\sigma_{e\perp}$	0.88	0.85
$\sigma_{e\parallel}$	1.65	1.65
asymmetricity	0.00	0.28

are listed in Table II and Table III, respectively. TEM and Gay-Berne parameters are selected to resemble the site–site model of Table III. In symmetric interaction models, all these models agree well in maximum well depths and separations. When the curves of the STEM are compared with those of the site–site model, the interaction strengths of the STEM are greater than those of the site–site model in the regions where the separation at maximum well depth of the STEM is less than those of the site–site model due to the shape differences. The site–site model is a spherocylinder while the STEM is an ellipsoid. As a special case, if we set $\sigma_{e\perp}$ and $\sigma_{e\parallel}$ to the side–side optimum distance and the end–end optimum distance, respectively, the STEM has the same potential as the Berne-Pechukas model.

In asymmetric interaction models, curves of the ATEM and the site–site model have similar trends. Some discrepancies between the curves of two models in this case may also be due to the shape differences as in the case of symmetric models.

3. MONTE CARLO SIMULATION

Generally, particles in the isotropic phase have 5 or 6 intermolecular degrees of freedom. The liquid crystal phase occurs with the loss of some degrees of freedom from the isotropic phase. The nematic phase occurs with the loss of rotational degrees of freedom from the isotropic phase. Components of ordering tensor for the molecular major axes with respect to an

TABLE II Parameters of the Gay-Berne model

	Symmetric
$\sigma_\perp$	1.00
$\sigma_\parallel$	3.00
μ	1.40
ν	0.35
$\varepsilon_e/\varepsilon_s$	0.14

TABLE III Parameters of the site–site models

SITE	*Symmetric* ε	*Asymmetric*$_e$	r
1	1.0	9.0	1.0
2	1.0	3.0	1.0
3	1.0	1.0	1.0
4	1.0	1.0	1.0
5	1.0	1.0	1.0

ensemble based coordinate system are [17]

$$Q_{\alpha\beta} = \left\langle \frac{1}{N} \sum_{j=1}^{N} \left(\frac{3}{2} u_{j\alpha} u_{j\beta} - \frac{1}{2} \delta_{\alpha\beta} \right) \right\rangle \tag{14}$$

where $\alpha, \beta = x, y, z$ coordinates and $u_{i\alpha}$ is the α component of $\mathbf{u}_i$ that is a unit vector of the major axis of the particle i. N is the number of particles and $\langle\rangle$ symbolizes a time average. When we diagonalize the Q matrix, the nematic order parameter, S, is obtained as the largest eigenvalue, and the nematic director is the corresponding eigenvector.

Radial distribution function (RDF) is frequently used for analysis of intermolecular distributions and appropriate when the potential representing particle is spherically equivalent. When a potential is not spherically equivalent, such as in liquid crystal molecules, the RDF yields ambiguous information. In the case of the liquid crystal molecule which is uniaxial, cylindrical distribution function (CDF) [3] is commonly used to analyze intermolecular distributions. In CDF, intermolecular distributions contain intermolecular distance and intermolecular orientation. CDF was divided into two, one with the acute angles and the other with the obtuse angles between two major axes, so that we may analyze parallel and antiparallel distributions of the nematic phase. Contour lines of CDFs were displayed from the density of 0.2 to 4.0 at intervals of 0.1.

The potential parameters used in MC simulations are defined as follows. The geometric ellipsoidal lengths of the major axis, $\sigma_{\parallel}$, and the minor axis, $\sigma_{\perp}$, are 3 and 1, respectively. The interaction ellipsoidal lengths of the major axis, $\sigma_{e\parallel}$, and the minor axis, $\sigma_{e\perp}$, are $0.9\sigma_{\perp}$ and $0.4\ \sigma_{\perp}$, respectively. The asymmetricity parameter of the ATEM is $0.36\sigma_{\perp}$ and the cut-off distance is

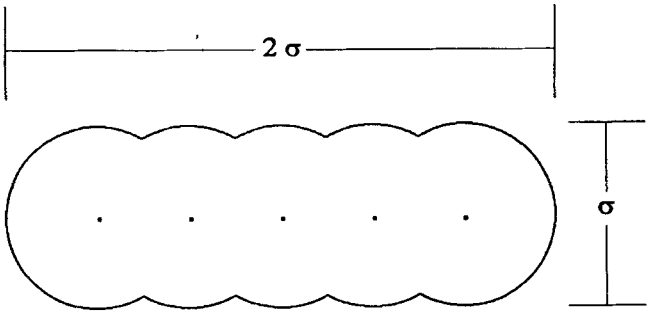

FIGURE 6 The site–site model having 5 interaction centers. The distance between neighboring centers is $\sigma/2$.

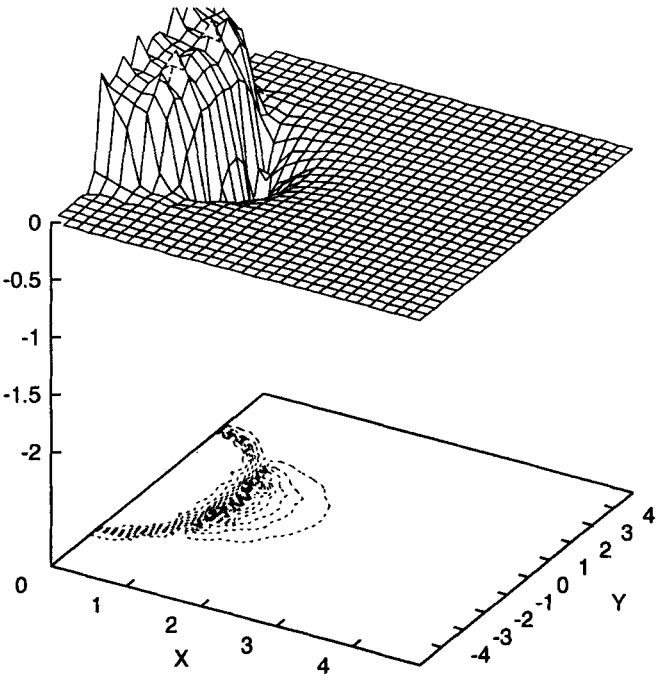

FIGURE 7 Potential energy surfaces of the STEM for the parallel orientation.

$4.0\sigma_0$. Potential energy surfaces of parallel and antiparallel orientations of the STEM and the ATEM are shown in Figure 7 and Figure 8. In these figures, the center of the geometry ellipsoid is located at (0,0) and the major axis of the particle is located on the +Y axis. We plot only the +X axis of the potential energy surfaces because the potential energies of TEMs are cylindrically symmetric. In the case of the STEM in Figure 7, the potential energy surfaces of parallel and antiparallel orientations are identical since the interaction potential of the STEM is symmetric along the major axis. The anisotropic geometry of an ellipsoidal form is visible in the repulsive domain, and anisotropic interactions can be seen by comparing the optimum interaction strengths of the side-by-side and end-by-end shapes. In the case of the ATEM shown in Figure 8, the center of the interaction ellipsoid is located at (0, asymmetricity parameter). Anisotropic geometry and interactions appear as in the case of the STEM. The plot of parallel orientation is similar to that of the STEM and omitted. Although the shape of the repulsive domain is similar to other cases for the antiparallel orientation of the ATEM, the shape of the optimum interaction strength is not symmetric along the Y axis as shown in Figure 8.

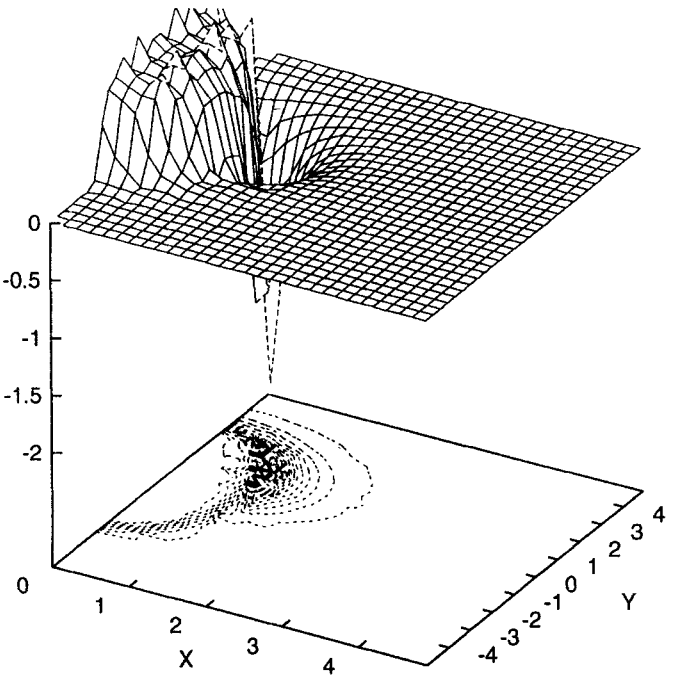

FIGURE 8 Potential energy surfaces of the ATEM for the antiparallel orientation.

The periodic boundary condition of rectangular box (V_x: V_y: V_z = 1:1:1.5) and NVT ensemble with 320 particles were used in MC simulations. The reduced density $\rho^* = N/V\sigma_0^3$ was chosen to be 0.3. Reduced temperature (T^*) is $K_\beta T/e_\times$ where $e_\times$ is the strength between two STEMs for the crossed shape. The same definition for T^* is used for ATEM. Initial melting temperature was chosen to be 3.0 T^* and the temperature was lowered by 10% in successive steps until the nematic phase formed. In the equilibration, we ran at least 30K Monte Carlo steps and performed more than 100K steps near the phase transition. After the equilibration, the averaging was performed with 10K steps. During the averaging run, bulk properties such as $\langle P_2 \rangle$, RDF and CDF were averaged at the end of every steps.

The variation of nematic order parameter $\langle P_2 \rangle$ is shown in Figure 9. The isotropicnematic phase transition temperatures of the STEM and the ATEM are probably higher than 1.0 T^*. The ATEM appears to have higher transition temperature than the STEM indicating that the asymmetricity of interactions could be a driving force to the nematic phase. This driving force does not seem to be very effective considering the substantial

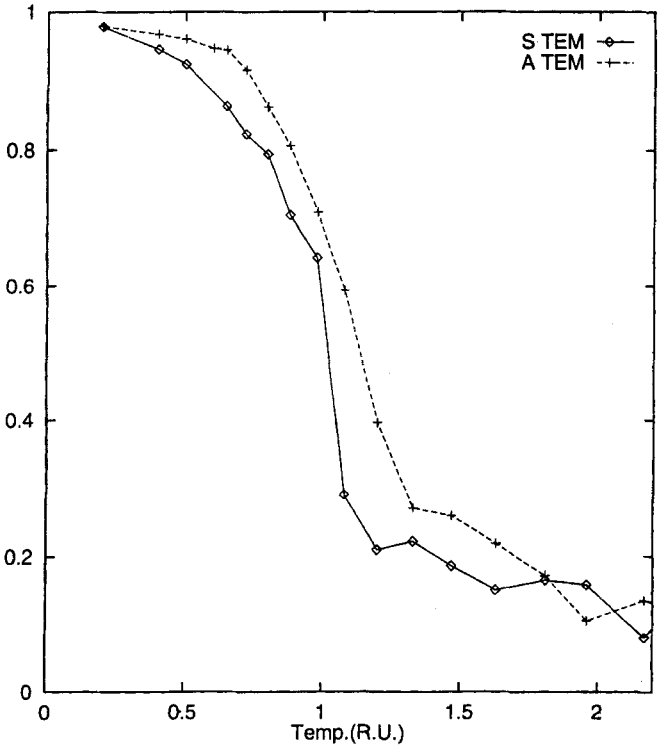

FIGURE 9 Order parameters as a function of reduced temperature T^*. The solid line is the order parameter of the STEM and the dashed line is that of the ATEM.

differences in potential energy surfaces between STEM and ATEM (Fig. 7 and 8).

RDFs and CDFs were obtained at the isotropic phase (2.17 T^*) and the nematic phase (0.72 T^*). We also divided RDF into two cases, one with acute angles between major axes of the pair and the other with obtuse angles as shown in Figures 10 and 11. When the phase becomes nematic, the RDF of acute angles becomes that of parallel orientations and the RDF of obtuse angles becomes that of antiparallel orientations. In the RDFs of the STEM and the ATEM, distributions of obtuse angles are less than those of acute angles, which are caused by the fluctuation of rotational distributions of major axes. As an example, let us consider the nematic phase having two rotational selectivity in the parallel and the antiparallel directions relative to the nematic director, when the fraction of particles having the same direction to the nematic director is α, then the fraction of particles with the reverse direction to the nematic director is $1 - \alpha$. The fraction of

the case in which an angle between major axes of two particles is an acute angle is $\alpha^2+(1-\alpha)^2$ and the fraction of the case in which an angle between major axes of two particles is an obtuse angle is $2\alpha(1-\alpha)$. Distributions of acute angles are equal to those of obtuse angles when α is 0.5 and greater than those of obtuse angles when α is not equal to 0.5. The fluctuation of rotational distributions of major axes increases in proportion to the simulation temperature. At the same temperature, deviation of distributions between acute angles and obtuse angles in the STEM is larger than that in the ATEM since particles of the STEM can rotate more easily than those of the ATEM.

RDFs of the isotropic phases (Fig. 10) of the STEM and the ATEM differ only slightly indicating that particles move easily to any point having negative interaction potential in the potential energy surface but not to the point having positive interaction potential energy. As a result, distributions depend not on interaction potentials but on geometric shapes. In the nematic phase of the STEM in Figure 11(a), the RDF of parallel orientation (or acute angle between two major axes) has the shape similar to the RDF of antiparallel orientation (or obtuse angle between two major axes), and shows local translational ordering with respect to the second neighbor. RDFs of the ATEM in Figure 11(b) are completely different from those of the STEM in Figure 11(a). The RDF of parallel orientations has maximum at the distance of about σ_0 but the RDF of antiparallel orientations has small distributions at that distance. In contrast, the RDF of antiparallel orientations has broad maximum distribution at about $3.0\sigma_0$ but the RDF of parallel orientations has its lowest distribution at that distance. These peak and valley of distributions are repeated at about $2.2\sigma_0$ intervals. Two particles located at the side-side optimum distance have parallel orientations relative to each other since negative interactions are possible in the side-side position near the distance of σ_0 only for the parallel orientations. The side-side position with an antiparallel orientation requires larger distance. Distributions of parallel and antiparallel orientations have positional periodicities as shown in Figure 11(b).

CDFs were averaged at every MC step during the production run and evaluated when the distance between two particles was less than $5.0\sigma_0$ distance. In Figures 12 and 13, the geometric center of a particle is located at (0,0) and the major axis of that particle is located on the +Y axis. The interaction center of a STEM is located at the same position of the geometric center and that of the ATEM is located at $(0, 0.36\sigma_0)$. We plot only the +X axis of each CDF because the potential energy of TEM is cylindrically symmetric. We also divide the CDF into one with acute angles and the

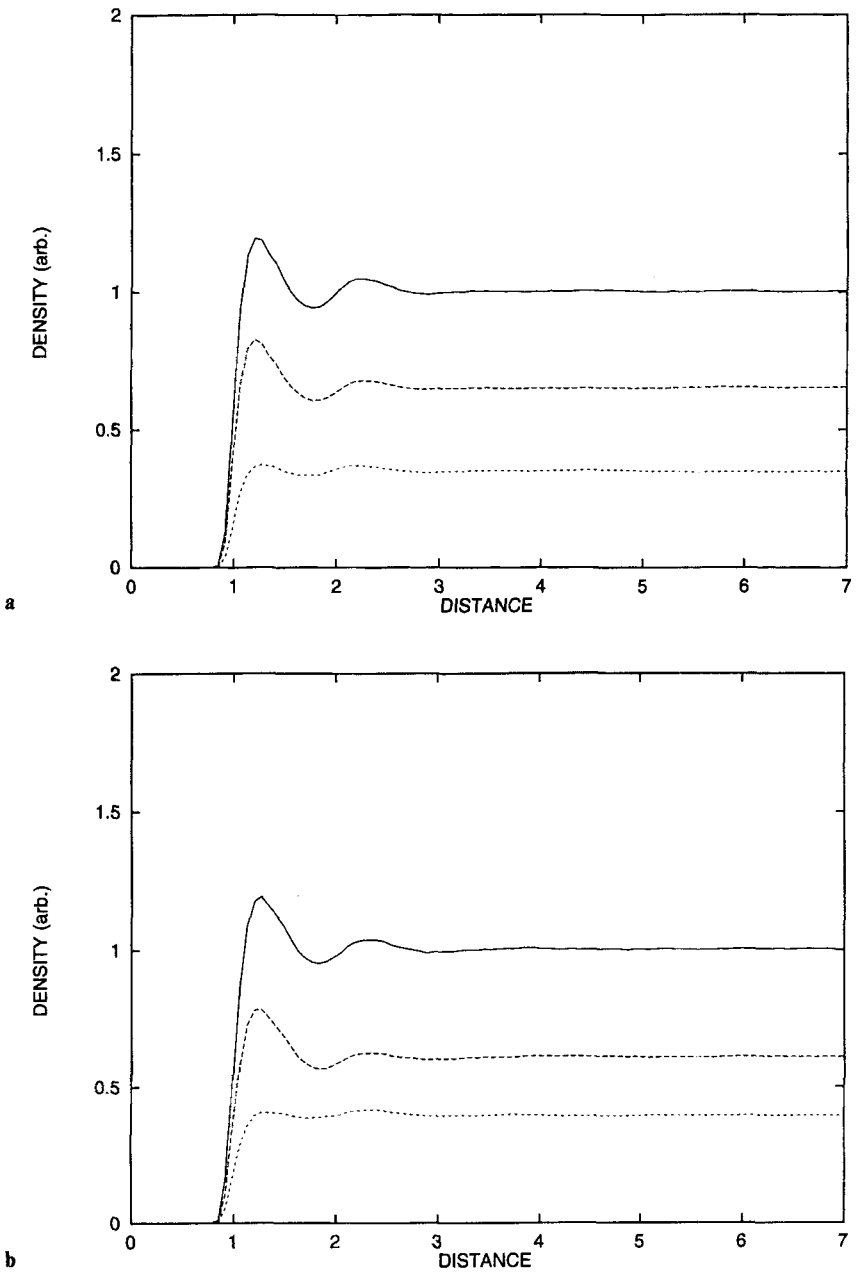

FIGURE 10 Radial distributions in the isotropic phase at $T^* = 2.17$. The dashed line is the radial distribution for the acute angles between two unit vectors, and the dotted line is that for the obtuse angles. The solid line is the sum of two distributions. (a) is for the STEM, and (b) is for the ATEM.

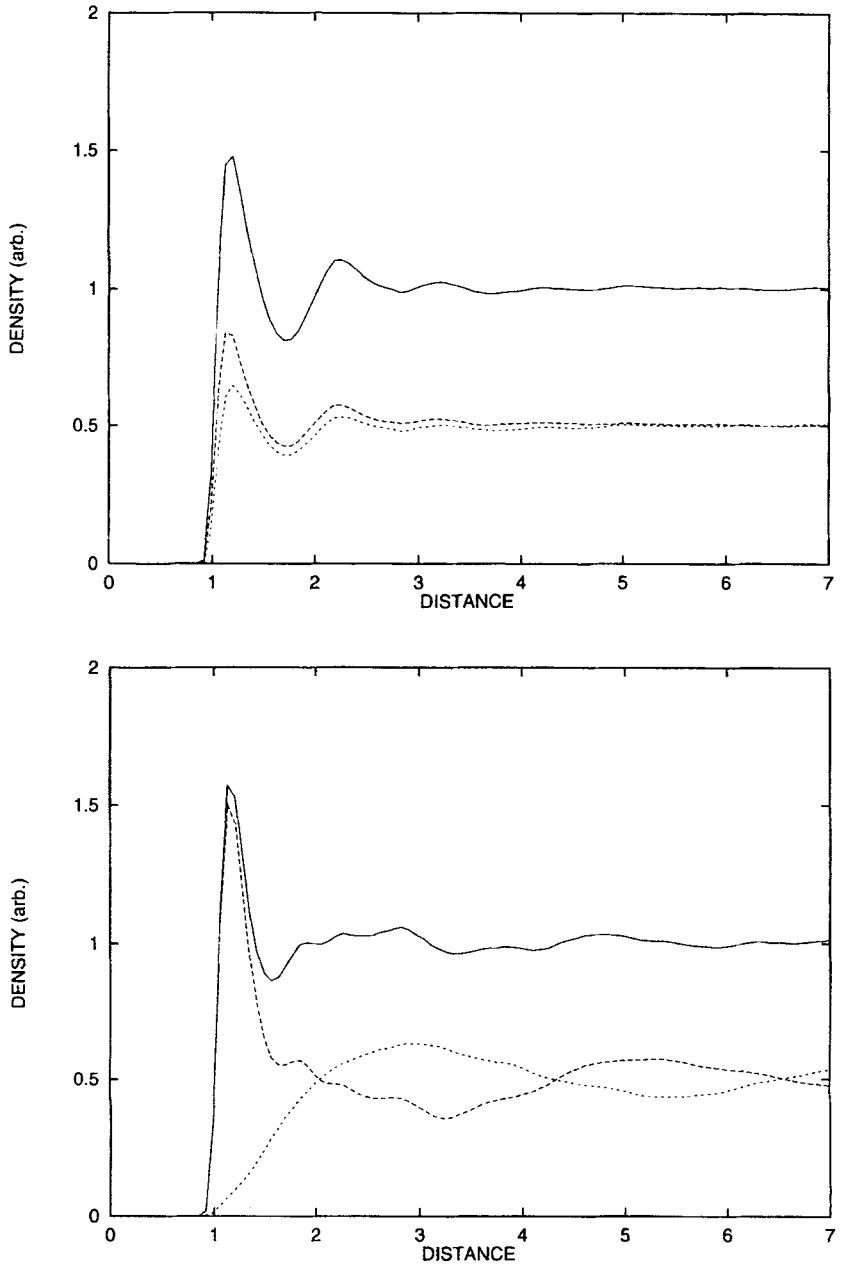

FIGURE 11 Radial distributions in the nematic phase at $T^* = 0.72$. The dashed line is the radial distribution for the acute angles between two unit vectors, and the dotted line is that for the obtuse angles. The solid line is the sum of two distributions. (a) is for the STEM, and (b) is for the ATEM.

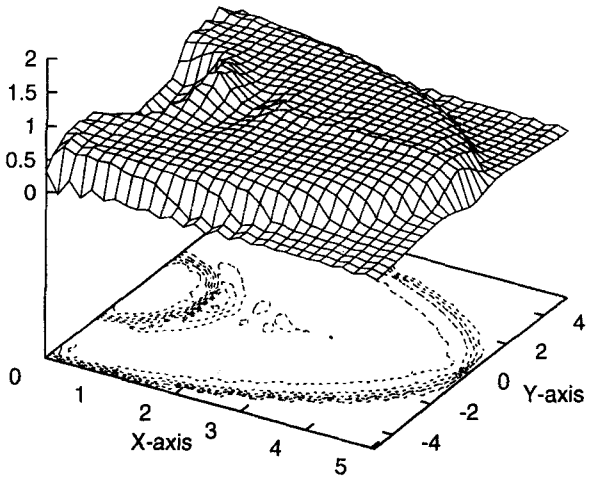

a

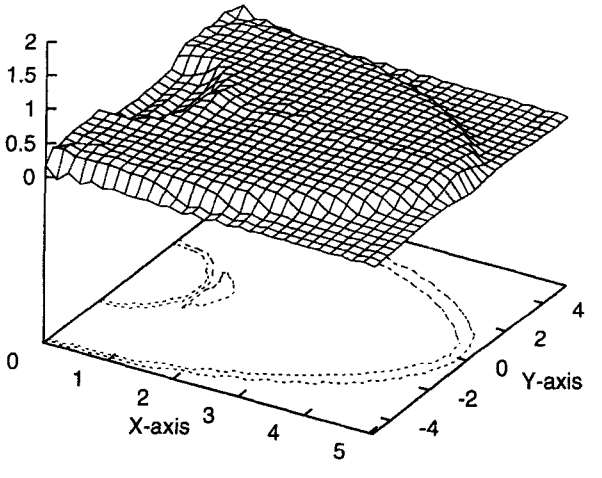

b

FIGURE 12 Cylindrical distributions in the isotropic phase at $T^* = 2.17$. (a) the acute angles between two unit vectors of STEMs, (b) the obtuse angle between two unit vectors of STEMs, (c) the acute angle between two unit vectors of ATEMs, (d) the obtuse angle between two unit vectors of ATEMs.

other with obtuse angles between two particles. As was explained for RDF, distributions of acute angles are greater than those of obtuse angles due to rotational fluctuations. In the isotropic phase shown in Figure 12, the CDF of the STEM is similar to that of the ATEM, and distributions of acute angles and obtuse angles have the same shape, indicating that distributions

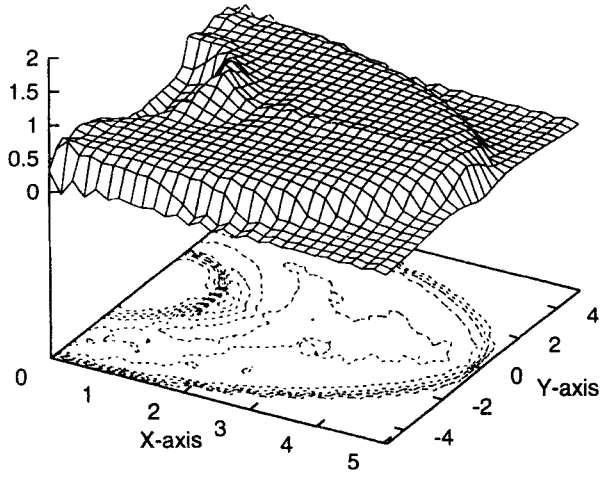

c

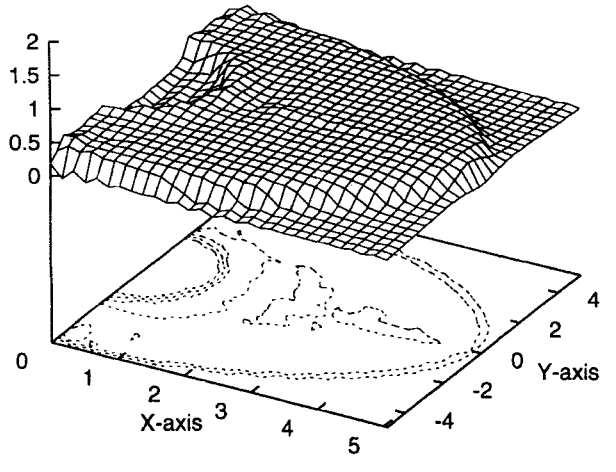

d

FIGURE 12 (*Continued*)

in the isotropic phase do not depend heavily on the interaction potential. In the nematic phase shown in Figure 13, CDFs of the STEM and the ATEM are different. In CDFs of the STEM in Figure 13(a) and (b), the distribution of the parallel and the antiparallel orientations have the same shape, and the maximum is located near the optimum distance of side–side position ($\simeq \sigma_0, 0.0$) due to the anisotropic interaction as shown in Figure 7. The distribution of the end–end position is not as flat as expected. The ridgeline of the end–end position extends parallel to the X axis, implying a local S_{A_1} phase.

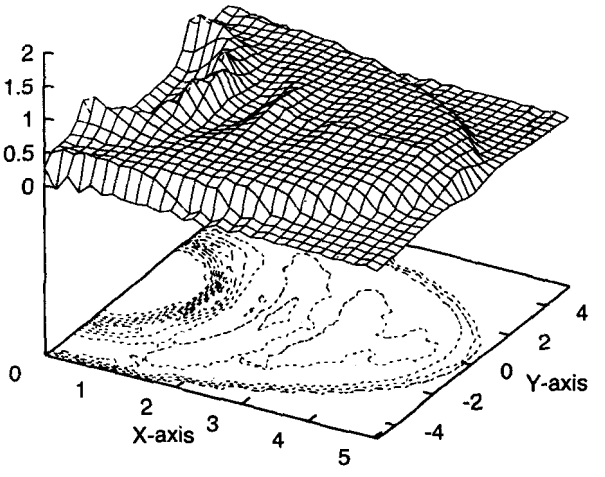

a

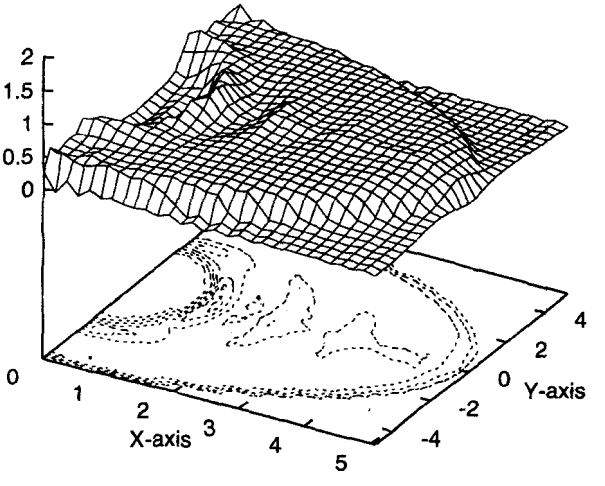

b

FIGURE 13 Cylindrical distributions in the nematic phase at $T^* = 0.72$, (a) the acute angles between two unit vectors of STEMs. (b) the obtuse angle between two unit vectors of STEMs. (c) the acute angle between two unit vectors of ATEMs, (d) the obtuse angle between two unit vectors of ATEMs.

In the case of the ATEM in Figure 13(c) and (d), the CDF of parallel orientations are totally different from that of antiparallel orientations. Distributions of parallel orientations show a ridgeline parallel to the X axis at the side–side position and the next ridgelines are separated by about $\pm 4.4\sigma_0$ along the Y axis as shown in Figure 13(c). The antiparallel orientation is

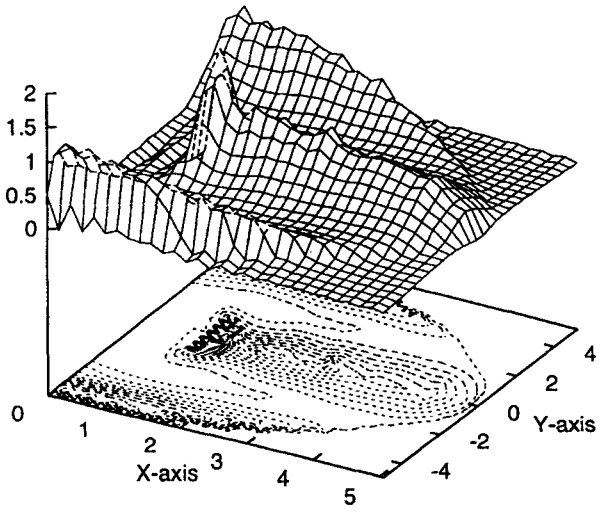

c

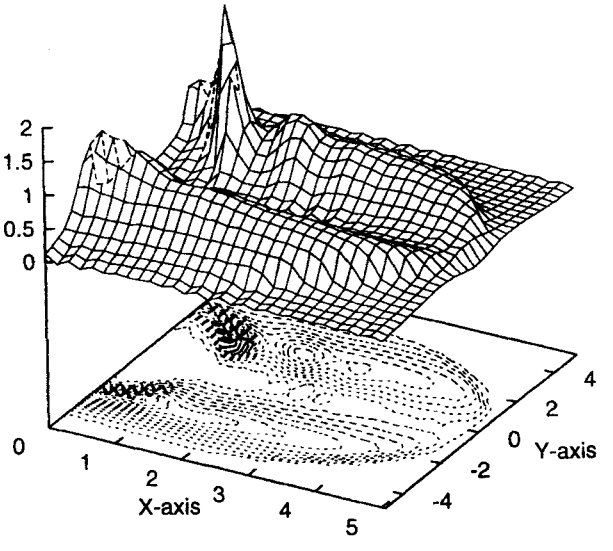

d

FIGURE 13 (*Continued*)

located between layers of parallel orientation as shown in Figure 13(d). The layer in the $+Y$ direction has varying distributions along the X direction, and has a maximum at $(0.88\sigma_0, 1.73\sigma_0)$ corresponding to an optimum position of the antiparallel interactions. This layer is separated by about $1.8\sigma_0$

toward the Y direction. The layer in the $-$ Y direction has a uniform distribution along the X direction, and this layer is separated by $2.5\sigma_0$ toward the $-$ Y direction. The layer in the $+$ Y direction has stronger interactions than the layer in the $-$ Y direction as can be seen in the potential energy surface of ATEM in Figure 8. The optimum distance of $3\sigma_0$ for the end–end direction implies that the layers of this phase are interdigitated. The layer in the + Y direction is more interdigitated than the layer in the $-$ Y direction suggesting that the driving factor to the interdigitated structure is the strong antiparallel pairing along the + Y direction. Despite the apparent layered structure, this phase is still nematic. The total distributions obtained by the summation of parallel and antiparallel distributions do not support a layered structure. The width of each layer needs to be narrower in order to be a true smectic phase (S_{Ad}).

4. CONCLUSION

In this paper, a TEM is proposed. This model uses two ellipsoids to describe a molecule: one ellipsoid represents the geometry and the other the interaction strengths of the molecule. Parameters σ and ε are obtained from the geometry ellipsoid and the interaction ellipsoid, respectively, by employing the Gaussian overlap concept. Common liquid crystal molecules may have asymmetric interactions along the major axis because of different atomic compositions and bond types. The present TEM can mimic this asymmetric interaction by separating the center of the interaction ellipsoid from that of the geometry ellipsoid. The maximum well depths and the separations at the maximum well depths of a STEM compare favorably with those of the corresponding Gay-Berne and the site–site models. Potential energy surfaces of an ATEM are also in good agreement with those of corresponding site–site model.

The NVT Monte Carlo simulation with 320 particles was performed for a STEM and an ATEM. RDFs and CDFs of the isotropic phase and the nematic phase were obtained. Distributions of STEM and ATEM in the isotropic phase are similar but those in the nematic phase are quite different. In the STEM, distributions of the parallel and the antiparallel orientations are similar to each other, and the side–side position is more favored than any other position. In the ATEM, the parallel orientation has the maximum distribution at the side–side position, while the antiparallel orientation has the maximum distribution at some distance off from the side–side direction. Distributions of these orientations indicate a layered

and interdigitated structure although total distributions do not support layered structures indicating that the phase is still nematic. ATEM displays a slightly higher transition temperature than STEM indicating that asymmetric interactions can be a driving force in a phase transition. It appears that the STEM and the ATEM can be useful in investigating the effect of asymmetric interactions in liquid crystal phases.

References

[1] Komolkin, A. V., Laaksonen, A. and Maliniak, A. (1994). "Molecular-dynamics simulation of a nematic liquid-crystal." *J. Chem. Phys.*, **101**, 4103.
[2] Glaser, M. A., Malzbender, R., Clark, N. A. and Walba, D. M. (1994). "Atomic-detail simulation studies of tilted smectics." *J. Phys.: Condens. Matter*, **6**, A261.
[3] Komolkin, A. V. and Maliniak, A. (1995). "Local structure in anisotropic systems determined by molecular dynamics simulation: Application to a nematic liquid crystal." *Mol. Phys.*, **84**, 1227.
[4] Cross, C. W. and Fung, B. M. (1994). "A simplified approach to molecular-dynamics simulations of liquid-crystals with atom-atom potentials." *J. Chem. Phys.*, **101**, 6839.
[5] Nicklas, K., Bopp, P. and Brickmann, J. (1994). "Computer-simulation studies of a model system for liquid-crystals consisting of semiflexible molecules." *J. Chem. Phys.*, **101**, 3157.
[6] Paolini, G. V., Ciccotti, G. and Ferrario, M. (1993). "Simulation of site-site soft-core liquid crystal models." *Mol. Phys.*, **80**, 297.
[7] Miguel, E., Rull, L. F., Chalam, M. K., Gubbins, K. E. and van Swol, F. (1991). "Location of the isotropic-nematic transition in the Gay-Berne model." *Mol. Phys.*, **72**, 593.
[8] Miguel, E. and Rull, L. F. (1992). "Dynamics of the Gay-Berne fluid." *Phys. Rev. A* **45**, 3813.
[9] Berardi, R., Emerson, A. P. J. and Zannoni, C. (1993). "Monte-Carlo investigations of a Gay-Berne liquid-crystal." *J. Chem. Soc. Faraday trans.*, **89**, 4069.
[10] Luckhurst, G. R. and Simmonds, P. S. J. (1993). "Computer-simulation studies of anisotropic systems 21. Parametrization of the Gay-Berne potential for model mesogens." *Mol. Phys.*, **80**, 233.
[11] Gay, J. G. and Berne, B. J. (1981). "Modification of the overap potential to mimic a linear site–site potential." *J. Chem. Phys.*, **74**, 3316.
[12] Sear, R. P. and Jackson, G. (1994). "Theory of hydrogen-bonding nematic liquid-crystals." *Mol. Phys.*, **82**, 473.
[13] Hashim, R., Luckhurst, G. R. and Romano, S. (1995). "Computer-simulation studies of anisotropic systems 24. Constant-pressure investigations of the smectic-B phase of the Gay-Berne mesogen." *J. Chem. Soc. Faraday trans.*, **91**, 2141.
[14] Ayton, G. and Patey, G. N. (1995). "A generalized gaussian overap model for fluids of anisotropic particles." *J. Chem. Phys.*, **102**, 9040.
[15] Berardi, R., Fava, C. and Zannoni, C. (1995). "A Gernaralized Gay-Berne intermolecular potential for biaxial particles." *Chem. Phys. Lett.*, **236**, 462.
[16] Berne, B. J. and Pechukas, P. (1972). "Gaussian model potentials for molecular interactions." *J. Chem. Phys.*, **56**, 4213.
[17] Chandrasekhar, S. (1977). "Statistical theories of nematic order." *Liquid Crystals* I. 14.